Coherent Scatterers Detection in Glacier Environments by means of TerraSAR-X Images

Maria J. Sanjuan-Ferrer[1], Irena Hajnsek[2,1], Kostantinos P. Papathanassiou[1]
[1)] German Aerospace Center (DLR), Microwaves and Radar Institute (HR), Germany
[2)] ETH Zurich, Institute of Environmental Engineering, Switzerland

Abstract

This paper investigates the detection of Coherent Scatterers (CSs) in Ice and Glacier terrain by means of TerraSAR-X images in the test case of the Helheim Glacier in Greenland. CSs are evaluated with respect to detection, properties and potential applications. The detection of CSs by means of TerraSAR-X data is discussed and optimised detection schemata for minimising false alarm rate are investigated. Properties and quality of the detected CSs are analysed.

1 Introduction

An important category of scatterers in SAR images are point (-like) scatterers. Their deterministic scattering behaviour combined with a high Signal to Noise Ratio (SNR) that usual characterizes this kind of scatterers makes them valuable for a wide spectrum of applications, ranging from image calibration to object characterization and information extraction.
A relevant class of point scatterers are the so called Coherent Scatterers (CSs) characterised by a stable spectral correlation. Accordingly, spectral correlation techniques have been proposed for their detection. The advantage of CSs compared to other point scatterers is that they can be estimated on a single image basis. The concept of CSs has been introduced and discussed in [2] where a first extensive analysis of their amplitude, polarimetric and interferometric properties has been performed on the basis of airborne data. Up to now, CSs detection has been investigated primarily in urban environments. In this work, the detection of CSs in terms of wide-band spaceborne SAR systems in natural scenarios, like ice and glacier terrain, is investigated and the properties of the detected CSs are analysed.

2 CSs Detection

Regarding the detection of CSs three different approaches have been proposed:

1. The originally proposed sublook coherence detection based on the cross-correlation of two spectral sub-bands [1][2].
2. The sublook entropy detection based on the cross-correlation of multiple spectral sub-bands that allows a more flexible detection with respect to the spectral characteristics of the individual CSs [1][2].
3. The phase variance approach that allows a widely preservation of the spatial resolution in the detection of CSs [3].

Each approach has his own pros and cons. However, common to all three approaches is the trade-off between spatial resolution (defined by the bandwidth of the individual sub-bands and the number of samples used) and the quality of the detected CSs.
The main problem in the detection of CSs in natural scenes lies in the fact that “natural” CSs are - in general - less deterministic than the ones detected in urban scenes. In order to be detected one needs to relax the estimation threshold. But this is linked to an increase of false alarm rate at the same time. The trade-off between number of detected CSs and at the same time the number of false alarms is in natural scenarios especially critical. In the following we will discuss ways to relax this trade-off.

3 CSs in Natural Environments

The test site considered is the Helheim glacier, located in the south-east of Greenland. It is one of the fastest glaciers of the world moving several kilometres per year. Our analysis is based on TerraSAR-X acquisitions performed between August 2008 and October 2009. The images were acquired every 11 days in the strip map mode, with a 150 MHz range bandwidth and incidence angle of 37.3°. The image acquired in the 19 of June 2009 is showed in Figure 1.
The method considered for the CSs detection in the present work is the phase variance approach. Ten

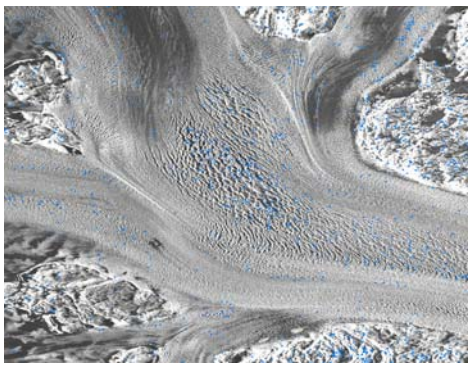

Figure 1 Detected CSs using the range spectrum and a threshold $\sigma^2_{rg} < 0.0009$ rad².

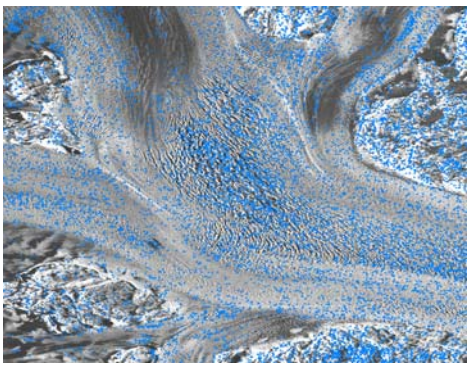

Figure 2 Detected CSs using the range spectrum and a threshold $\sigma^2_{rg} < 0.0025$ rad².

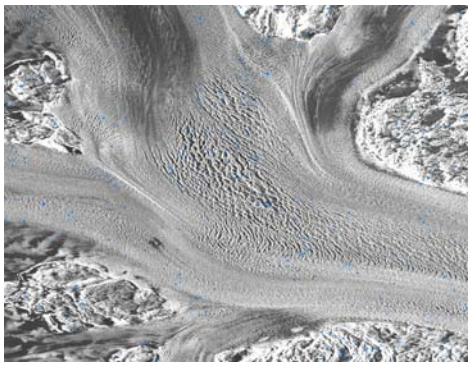

Figure 3 Detected CSs using the azimuth spectrum and a threshold $\sigma^2_{az} < 0.0009$ rad².

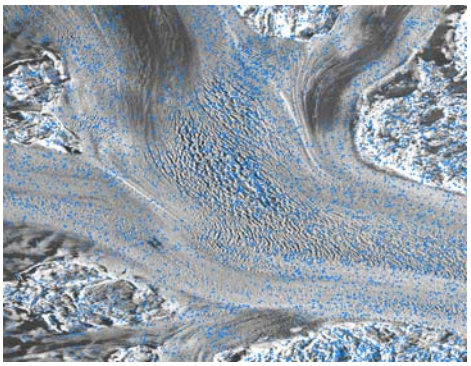

Figure 4 Detected CSs using the azimuth spectrum and a threshold $\sigma^2_{az} < 0.0025$ rad².

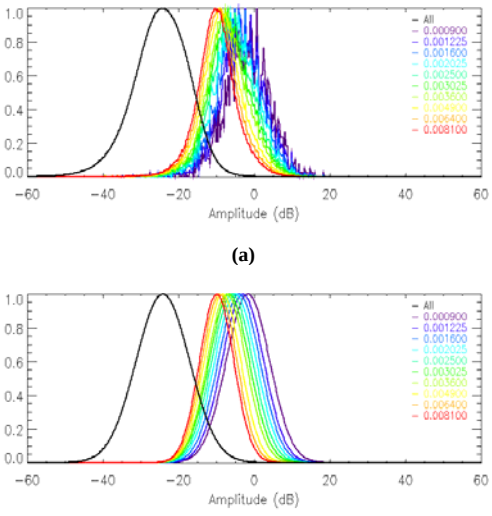

(a)

(b)

Figure 5 (a): Normalized amplitude histograms for the background scene (black) and the detected CSs in range for different thresholds (colored). (b): Corresponding Gaussian approximation of the amplitude histograms.

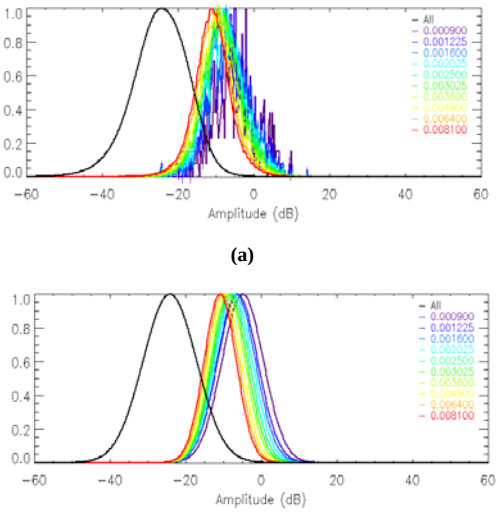

(a)

(b)

Figure 6 (a): Normalized amplitude histograms for the background scene (black) and the detected CSs in azimuth for different thresholds (colored). (b): Corresponding Gaussian approximation of the amplitude histograms.

sublooks of 60 MHz each out of the available 150 MHz have been generated, spanning a frequency range of 90 MHz. The phase derivative variance σ^2 has been computed for every pixel across these 10 sublooks. Pixels with $\sigma^2 < 0.0009$ rad² were interpreted as CSs and they are plotted in Figure 1. The CSs detected using a higher threshold are shown in Figure 2. In this case, pixels with $\sigma^2 < 0.0025$ rad² were considered as CSs.

In a second step, the detection has been performed in azimuth. 10 sublooks of 1106 Hz each out of the 2765 Hz azimuth available bandwidth have been formed and the variance σ^2 of the phase derivative for every pixel across these 10 looks is estimated. Figure 3 shows the azimuth detection for $\sigma^2 < 0.0009$ rad² and Figure 4 the azimuth detection for $\sigma^2 < 0.0025$ rad². A plot of the normalized amplitude histogram for the background scene (black) and the CSs detected in range for different thresholds (colored) is shown on Figure 5 (a). In order to facilitate the evaluation of the distribution plots, the histograms are approximated by Gaussian distributions as shown in Figure 5 (b). One can see that the Signal to Clutter Ratio (SCR) increases with decreasing phase derivative variance threshold. Equivalent plots for the case of azimuth detection are shown in Figure 6.

In Figure 7, examples of the range (top) and azimuth (bottom) normalized amplitude profiles of some of the detected CSs are plotted indicating the point-like response of the detected CSs in both directions.

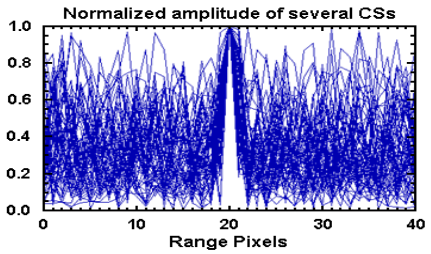

(a)

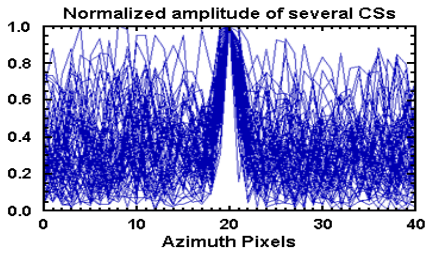

(b)

Figure 7 Normalized amplitude profiles of the detected CSs. (a): in range. (b): in azimuth.

4 Detection Problem: SCR, PD and PFA

The SCR defines the phase stability of the detected CSs. Considering a resolution cell which contains only a single CS in clutter, the power of the point (-like) scatter is $|\mu|^2$ and the variance of the clutter (and noise) is σ^2. So, SCR is $|\mu|^2 / \sigma^2$. Using the Central Limit Theorem (CLT), for a large number of clutter sources, the return tends to a complex circular Gaussian distribution, with mean μ and variance σ^2. That distribution has its real and imaginary components uncorrelated with equal variance ($\sigma^2_{real} = \sigma^2_{imag}$), i.e., it has a Rayleigh distributed amplitude and uniform distributed phase with amplitude and phase being uncorrelated [4].

If a Taylor series expansion is used, the phase variance of the return, σ_ϕ^2, can be approximated by:

$$\sigma_\phi^2 \cong \frac{\sigma^2}{2|\mu|^2} = \frac{1}{2SCR} \qquad (1)$$

when the SCR is high enough.

The amplitude of the return tends to a Gaussian distribution when the SCR increases:

$$f_A(a) \to N(|\mu|, \frac{\sigma^2}{2}) \text{ as } \sqrt{SCR} = \frac{|\mu|}{\sigma} \to \infty \qquad (2)$$

with the approximation being valid for SCR > 8 (9 dB) [4][5]. Note that according to Equation (2) the width of the distribution is independent of the SCR.

Fixing a threshold to distinguish between a resolution cell with a single CS in clutter and one with only clutter (in our case, the detection threshold used is the phase derivative variance, and it's related with this threshold), it's possible to calculate the Probability of Detection (PD) and the Probability of False Alarm (PFA) [6].

5 Detection Analysis

In this section, the combined range and azimuth CSs detection is addressed. First, the potential of using azimuth spectral correlation to improve CSs detection in range - in terms of higher SCR and a reduced false alarm rate - is evaluated. A comparison between range, azimuth and common (i.e. range and azimuth) detection is performed.

5.1 Improvement of Range Detection using Azimuth Information

In order to improve the SCR at the more relaxed thresholds, a combination of range and azimuth spectral information is performed. For this:

1. 10 sublooks of 60 MHz each out of the available 150 MHz range bandwidth have been formed and the variance σ^2 of the phase derivative for every pixel across these 10 looks is estimated.
2. CSs are detected for a given range threshold (σ^2 = 0.0009 and 0.0081 rad²).
3. 10 sublooks of 1106 Hz each out of the 2765 Hz azimuth bandwidth have been formed and the variance of the phase derivative for every pixel across these 10 looks is estimated.
4. From the CSs detected in range, the ones that have an azimuthal variance $\sigma^2 < 0.0016$ rad² are selected.

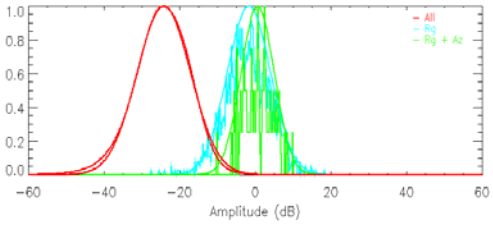

(a)

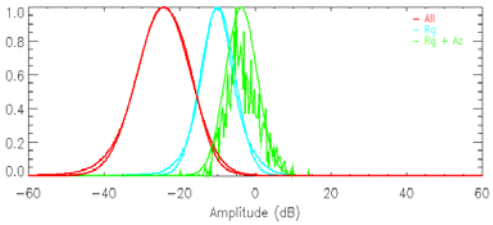

(b)

Figure 8 Normalized amplitude histograms of all pixels - including CSs - (red), CSs detected in range (blue) and CSs detected using range and azimuth (green). (a): range threshold σ^2_{rg}=0.0009 rad²; range threshold σ^2_{rg}=0.0009 and azimuth threshold σ^2_{az}=0.0016 rad². (b): range threshold σ^2_{rg}=0.0081 rad²; range threshold σ^2_{rg}=0.0081 and azimuth threshold σ^2_{az}=0.0016 rad².

The obtained results in terms of SCR are shown in Figure 8. In the first case, when the more restricted range threshold is used (σ^2 = 0.0009 rad²), the SCR improvement after applying the azimuthal filter is about 2 dB. In the second case, with the more relaxed range threshold (σ^2 = 0.0081 rad²), the SCR improvement is almost 6 dB.

5.2 Detection in common

In this section, a comparison between range only, azimuth only and common range-azimuth detection is addressed. The detection of CSs is performed by forming:

1. In range, 10 sublooks of 60MHz each out of the available 150 MHz azimuth bandwidth, covering a frequency range of 90 MHz.
2. In azimuth, 10 sublooks of 1106 Hz each out of the available 2765 Hz azimuth bandwidth, covering a frequency range of 1659 Hz.

In this way, for the common detection, only the CSs that have a phase derivative variance σ^2 less than a given threshold in both directions (range and azimuth) are considered as detected CSs.
Figure 9 shows a table with a comparison between the CSs detection in range only, azimuth only and commonly in range and azimuth. The two phase variance threshold used are σ^2 = 0.0016 and 0.0049 rad². The number of detected points in range is higher than in the other cases, but the commonly in range and in azimuth ones have a better quality in terms of SCR.

		NDP	*SCR (dB)*
RG	$\sigma^2_{rg} < 0.0016$ rad²	5586	20.16
	$\sigma^2_{rg} < 0.0049$ rad²	69789	15.81
AZ	$\sigma^2_{az} < 0.0016$ rad²	1898	17.54
	$\sigma^2_{az} < 0.0049$ rad²	40433	14.55
COM	$\sigma^2_{com} < 0.0016$ rad²	176	23.60
	$\sigma^2_{com} < 0.0049$ rad²	4830	19.71

Figure 9 Table with a comparison between the CSs detection in range only, azimuth only and commonly in range and azimuth, for two different thresholds. The two parameters calculated are the Number of Detected Points (NDP) and the Signal to Clutter Ratio (SCR).

6 Conclusions

The detection of Coherent Scatterers (CSs) in glacier environments has been evaluated. The approach considered is the phase variance method [3], which exploits the high phase stability characteristic of the CSs along the frequency and independently of the direction (range or azimuth).
The potential of the common (in range and in azimuth) CSs detection in natural scenes in order to suppress false alarms has been discussed.

References

[1] R. Zandona-Schneider, K. P. Papathanassiou, I. Hajnsek and A. Moreira: *Analysis of Coherent Scatterers over Urban Areas.* POLinSAR'2005, Frascati, Italy, January 2005.

[2] R. Zandona-Schneider, K. P. Papathanassiou, I. Hajnsek and A. Moreira: *Polarimetric and Interferometric Characterization of Coherent Scatterers in Urban Areas*. IEEE Trans. Geoscience and Remote Sensing, vol. 44, No. 4, April 2006.

[3] R. Zandona-Schneider and K. P. Papathanassiou: *Estimation and Correction of Ionospheric Induced Phase Errors in SAR images using Coherent Scatterers*. IGARSS'09, Cape Town, South Africa, July 2009.

[4] R. Brcic, M. Eineder, K. P. Papathanassiou and R. Zandona-Schneider: *D6 - Technical Note on PS Detection and Comparison with Standard PSI.* Project: Wideband SAR Interferometry, ESA Contract, September 2009.

[5] N. Adam, B. Kampes and M. Eineder: *Development of a Scientific Permanent Scatterer System: Modifications for Mixed ERS/Envisat Time Series.* 2004 Envisat & ERS Symposium, Salzburg, Austria, September 2004.

[6] M. Barkat: *Signal Detection and Estimation*, Artech House, ISBN 1-58053-070-2.